

# The land of deformation south of $^{68}\text{Ni}$

S. M. Lenzi,<sup>1</sup> F. Nowacki,<sup>2</sup> A. Poves,<sup>3</sup> and K. Sieja<sup>2</sup>

<sup>1</sup>*Dipartimento di Fisica dell'Università and INFN, Sezione di Padova, I-35131 Padova, Italy*

<sup>2</sup>*IPHC, IN2P3-CNRS et Université de Strasbourg, F-67037 Strasbourg, France*

<sup>3</sup>*Departamento de Física Teórica e IFT-UAM/CSIC,*

*Universidad Autónoma de Madrid, E-28049 Madrid, Spain*

(Dated: January 12, 2021)

We study the development of collectivity in the neutron-rich nuclei around  $N = 40$ , where experimental and theoretical evidences suggest a rapid shape change from the spherical to the rotational regime, in analogy to what happens at the *island of inversion* surrounding  $^{31}\text{Na}$ . Theoretical calculations are performed within the interacting shell model framework in a large valence space, based on a  $^{48}\text{Ca}$  core which encompasses the full  $pf$  shell for the protons and the  $0f_{5/2}$ ,  $1p_{3/2}$ ,  $1p_{1/2}$ ,  $0g_{9/2}$  and  $1d_{5/2}$  orbits for the neutrons. The effective interaction is based on a G-matrix obtained from a realistic nucleon-nucleon potential whose monopole part is corrected empirically to produce effective single particle energies compatible with the experimental data. We find a good agreement between the theoretical results and the available experimental data. We predict the onset of deformation at different neutron numbers for the various isotopic chains. The maximum collectivity occurs in the chromium isotopes, where the large deformation regime starts already at  $N = 38$ . The shell evolution responsible for the observed shape changes is discussed in detail, in parallel to the situation in the  $N = 20$  region.

PACS numbers: 21.60.Cs, 21.10.-k, 21.10.Re

## I. INTRODUCTION

In the last decades, more and more experimental evidence has been accumulated establishing the breaking of the shell closures known at the stability valley when approaching the drip lines, mainly at the very neutron-rich side. The first example of an unexpected disappearance of a shell closure ( $N = 8$ ) was found in  $^{11}\text{Be}$ , whose ground state is an intruder  $1/2^+$  located 320 keV below the "natural"  $0\hbar\omega$   $1/2^-$  state [1]. However, the true relevance of this finding was not recognized till many years later, and even now it is shadowed by the fame of its more neutron-rich isobar  $^{11}\text{Li}$ . In the  $sd$  shell, the expected  $N = 20$  semi-magic neutron rich nuclei turned out to be actually well deformed [2, 3]. The presence of deformed ground states in the nuclei around  $^{32}\text{Mg}$  and the breaking of the  $N = 20$  shell closure in this region has been extensively studied experimentally and theoretically (see [4–6] for shell model reviews). The aim of these studies is to map the limits of the so-called *island of inversion*, i.e. the region of nuclei where the strong quadrupole correlations overcome the spherical mean-field gaps, favoring energetically the deformed intruders, which often become ground states. Indeed, another basic aim is to understand microscopically the dynamics responsible for these shape transitions.

The question of the persistence of the  $N = 40$  harmonic oscillator closure in neutron-rich nuclei comes in naturally in this context. The high lying  $2^+$  state observed in  $^{68}\text{Ni}$  and its low  $B(E2; 2^+ \rightarrow 0^+)$  value are the result of the relatively large energy gap separating the  $pf$  and  $0g_{9/2}$  orbitals [7]. However, this gap gets reduced (or even disappears) when protons are removed from  $^{68}\text{Ni}$ : The nucleus  $^{66}\text{Fe}$ , with only two protons less,

shows a sudden change in nuclear structure with an increased collectivity manifested via its very low lying  $2^+$  state. Along the iron chain, indications for a collective behavior come from the systematics of the  $2^+$  states [8] as well as from the recent measurement of the  $B(E2)$  values in  $^{64,66}\text{Fe}$  [9, 10]. The evolution of the  $B(E2)$  values in iron isotopes points to a sudden increase of collectivity when approaching  $N = 40$ . Only very recently the first measurement of the excited levels in  $^{64}\text{Cr}$  has been reported [11]. This is the nucleus where theoretical calculations predicted the lowest lying  $2^+$  level in the region [12–14]. The measured  $2^+$  state energy agrees within 100 keV with those theoretical predictions. The sudden shape change at  $N = 40$  challenges the theoretical models, which have to account for a particularly rapid shell evolution responsible for these effects. Recent beyond mean-field HFB+GCM calculations with the Gogny force, reported in Ref. [15], show an increase of collectivity towards the proton drip line. The spherical neutron single-particle energies obtained in the HFB approach reveal almost no variation of the  $N = 40$  gap with the proton number between  $Z = 20$  and  $Z = 28$ . As a consequence, only a moderate collectivity in the iron and chromium chains is found, without visible structure changes between them. The collectivity at  $N = 40$  has been previously a subject of many shell model studies using different valence spaces and interactions [11–14, 16]. In particular, it has been shown that the shell model calculations using the  $0f_{5/2}$ ,  $1p_{3/2}$ ,  $1p_{1/2}$ ,  $0g_{9/2}$  neutron orbitals (the  $fpg$  valence space) and realistic interactions [13], can reproduce rather well the level schemes of  $^{62,64}\text{Fe}$ , but fail to do so for the  $2^+$  state of  $^{66}\text{Fe}$  [16]. To reproduce the large quadrupole collectivity in this mass region, the inclusion of the neutron  $1d_{5/2}$  orbital is needed, as first

surmised in Ref. [12] and confirmed recently in Ref. [9]. This can be explained in terms of the quasi-SU3 approximate symmetry: In this framework, the deformation is generated by the interplay between the quadrupole force and the central field in the subspace consisting on the lowest  $\Delta j = 2$  orbitals of a major shell [17].

In this work we discuss in detail how the sudden onset of collectivity can be interpreted in terms of shell model calculations in large model spaces and we look for the similarities in the deformation-driving mechanisms at  $N = 20$  and  $N = 40$  when approaching the neutron drip line. We present novel calculations for the  $N = 40$  region, in a model space including the  $pf$ -shell for protons and the  $0f_{5/2}$ ,  $1p_{3/2}$ ,  $1p_{1/2}$ ,  $0g_{9/2}$  and  $1d_{5/2}$  orbits for neutrons. We discuss first our model space and interaction as well as the computational details in Sec. II. The shape evolution along the  $N = 40$  line is studied in Section III. Next, we illustrate the development of deformation along the isotopic chains of iron and chromium in Sec. IV and we discuss the structure of the nickel isotopes. Conclusions are given in Sec. V.

## II. THE VALENCE SPACE

The physics of the  $N = 40$  nuclei has been discussed in the recent past both experimentally and theoretically [5, 8, 9, 11–16]. In  $^{68}\text{Ni}$ , the  $N = 40$  harmonic oscillator shell closure is somewhat weakened, however, whereas some of its properties seem consistent with a superfluid behavior, others may point to a double magic character. Below  $^{68}\text{Ni}$ , the iron and chromium isotopic chains are characterized by an open proton shell which favors the development of quadrupole correlations. Such a situation occurs also for the  $N = 20$  nuclei in the so called *island of inversion* around  $^{32}\text{Mg}$  [18]: the protons occupy the  $N = 2$  harmonic oscillator shell and the neutrons may lie either in the  $N = 2$  harmonic oscillator shell (normal filling) or in the  $1p_{3/2}$  and  $0f_{7/2}$  orbitals from the  $N = 3$  major shell (intruder configurations). The latter orbits form a quasi-SU3 block [19] which enhances the quadrupole correlations. Extended shell model calculations by the Tokyo group, with the SDPF-M effective interaction [18], predict the dominance of different type of configurations (0p0h, 1p1h, 2p2h) for the ground states of the nuclei with  $18 \leq N \leq 22$  and  $10 \leq Z \leq 14$ , delineating the contours of the island of inversion.

To assess if such a scenario could develop around  $^{68}\text{Ni}$ , we adopt here a model space based on a  $^{48}\text{Ca}$  core which comprises the  $pf$ -shell for protons and the  $1p_{3/2}$ ,  $1p_{1/2}$ ,  $0f_{5/2}$ ,  $0g_{9/2}$ , and  $1d_{5/2}$  orbits for neutrons. The degrees of freedom that can be encompassed in this valence space are very similar to the ones present in the study recalled previously [18], and the same kind of phenomena could therefore be described. The advantage of this valence space is that it contains all the physical degrees of freedom important for the description of the low-lying properties of these nuclei, it is computationally tractable, (see

precisions hereafter) and it is almost free of center of mass spuriousity since its main components, the  $0f_{7/2} \rightarrow 0g_{9/2}$  excitations, are excluded from the space.

The interaction proposed in this work, denoted hereafter LNPS, is a hybrid one, based on several sets of realistic two-body matrix elements (TBME). Its main building blocks are:

- The last evolution of the Kuo-Brown interaction (KB3gr) for the  $pf$ -shell [20];
- The renormalized  $G$ -matrix of Ref. [21] with the monopole corrections introduced in [22], for the remaining matrix elements involving the  $1p_{3/2}$ ,  $1p_{1/2}$ ,  $0f_{5/2}$ , and  $0g_{9/2}$  neutron orbits.
- The  $G$ -matrix based on the Kahana-Lee-Scott potential [23], for the matrix elements involving the  $1d_{5/2}$  orbit. This potential has been successfully employed in the definition of the recent SDPF-U shell model interaction [24] for the description of neutron-rich  $sd - pf$  nuclei.

In addition, another set of experimental constraints has been taken into account for the final tuning of the monopole Hamiltonian:

- The  $Z = 28$  proton gap around  $^{78}\text{Ni}$  is inferred from recent experimental data in  $^{80}\text{Zn}$  and fixed so as to reproduce the measured  $B(E2)$ . A standard polarization charge of  $0.5e$  has been used in all the calculations presented in this work.
- The size of the  $N = 50$  neutron gap in  $^{78}\text{Ni}$  has been estimated to be  $\sim 5$  MeV. The evolution of the neutron gap with the neutron number is rather independent on the proton number. On the contrary, the systematics [25] shows that the  $0g_{9/2} - 1d_{5/2}$  gap in Zr isotopes increases by 3 MeV when the neutron  $0g_{9/2}$  orbital is filled. We assume a similar behavior for the Ni chain. With this assumption, the observed  $5^+$ ,  $6^+$  states in  $^{82}\text{Ge}$ , which are supposed to be 1p-1h excitations across the  $N = 50$  gap, are correctly reproduced [26].

Finally, in order to compensate for the absence in our space of the third member of the quasi-SU3 sequence, the  $2s_{1/2}$  neutron orbit, we have increased the quadrupole-quadrupole interaction of the neutron  $0g_{9/2}$  and  $1d_{5/2}$  orbits by 20%.

The effective single particle energies (ESPE) of the LNPS interaction are shown in Fig. 1 for the neutron orbits at  $N = 40$ , between  $^{60}\text{Ca}$  and  $^{72}\text{Ge}$ . For comparison, we show in the same figure the neutron ESPE at  $N = 20$  between  $^{28}\text{O}$  and  $^{36}\text{S}$ , calculated with the SDPF-U interaction [24]. The similarities are striking. In the  $N = 20$  case, a reduction of the neutron  $0d_{3/2} - 0f_{7/2}$  gap takes place when protons are removed from the proton  $0d_{5/2}$  orbital. This feature, accompanied by the proximity of the quadrupole partner neutron orbitals  $0f_{7/2}$  and  $1p_{3/2}$ ,

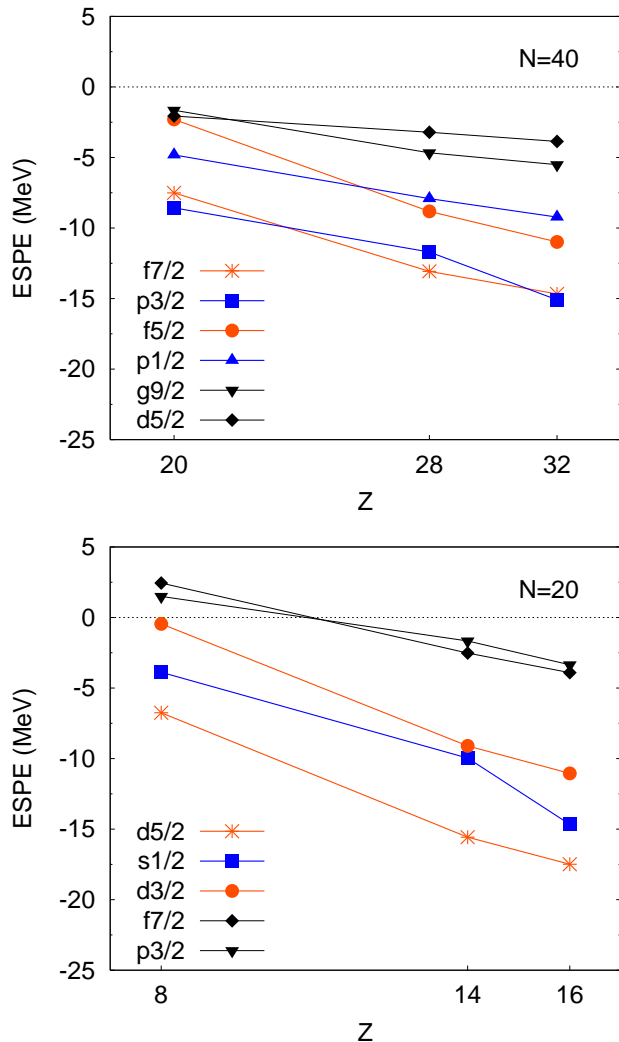


FIG. 1: (Color online) Neutron effective single particle energies obtained with the LNPS interaction at  $N = 40$  (upper part) and with the SDPF-U interaction at  $N = 20$  (lower part).

is responsible for the formation of the *island of inversion* at  $N = 20$ . At  $N = 40$  one observes the same behavior but for the neutron  $0f_{5/2} - 0g_{9/2}$  gap when going down from  $^{68}\text{Ni}$  and the closeness of the quadrupole partners  $0g_{9/2} - 1d_{5/2}$ .

The analogy in the shell evolution between  $N = 20$  and  $N = 40$  suggests therefore a possibility of another *island of inversion* below  $^{68}\text{Ni}$ .

As mentioned already, the deformation driving role of the neutron  $1d_{5/2}$  orbital below  $^{68}\text{Ni}$  was already discussed in the shell model calculations of Ref. [12]. However, due to the computational limitations at that time, the calculations were performed with a closed neutron  $1p_{3/2}$  orbit, therefore using  $^{52}\text{Ca}$  as a core. This is no longer an issue here: The present calculations have been carried out including up to 14 particle-14 hole excitations

across the  $Z = 28$  and  $N = 40$  gaps, when it appeared necessary to assure the convergence of the calculated electromagnetic properties. The largest dimensions of the matrices treated here reach  $10^{10}$  in the case of  $^{64}\text{Fe}$ . All the calculations of this work have been performed using the m-scheme shell model code ANTOINE [27].

### III. THE PROPERTIES OF THE $N = 40$ ISOTONES FOR $Z \leq 28$ AND THE NEW REGION OF DEFORMATION

The change of structure in even-even  $N = 40$  isotones from  $^{68}\text{Ni}$  down to  $^{60}\text{Ca}$  is illustrated in Fig. 2. In part (a) the evolution of the excitation energy of the  $2^+$  state is plotted while part (b) shows the corresponding evolution of the  $E2$  transition rates. The available experimental data are satisfactorily reproduced in all cases. Our theoretical approach predicts the maximal deformation at the middle of the proton shell, i.e. in  $^{64}\text{Cr}$ , where the calculated  $2^+$  energy is the lowest and the value of the  $B(E2; 2^+ \rightarrow 0^+)$  is the largest.

In Table I we list the extra occupancies of the two neutron intruder orbitals,  $0g_{9/2}$  and  $1d_{5/2}$ , relative to the normal filling. The occupation of the  $0g_{9/2}$  orbit in  $^{68}\text{Ni}$  is close to 1, which corresponds to  $\approx 50\%$  of the calculated wave function having a  $J = 0$  pair excited across  $N = 40$  gap. The wave function is however difficult to interpret, because, in spite of its very large content of excited pairs, the doubly magic component is still substantial. This is probably the reason why  $^{68}\text{Ni}$  shows at the same time an increase of the  $2^+$  excitation energy typical for doubly magic nuclei, and no sign of shell closure in the neutron separation energy.

The occupation of both neutron intruder orbits grows rapidly when protons are removed, due to the reduction of the neutron  $N = 40$  gap shown in Fig. 1. The ratio of the  $0g_{9/2}$  to  $1d_{5/2}$  occupations also evolves from Ni to Ca, partly as an effect of the level crossing taking place around  $^{62}\text{Ti}$ , but mostly due to the quasi-SU3 structure of the intruder states. The very important role of the  $1d_{5/2}$  neutron orbit in the build up of collectivity in this region sheds doubts about the results of Ref. [14], which do not include this orbit. The more so when one examines the very unrealistic ESPE that they enforce into their schematic interaction in order to get results close to the experimental data.

In Table I we list as well the percentages of neutron n-particle n-hole excitations in the ground state wave functions. The 4p-4h components are dominant in Fe, Cr, Ti and Ca, however 2p-2h and 6p-6h contributions are sizable. The complexity of the wave functions constitutes the main difference between  $N = 40$  and  $N = 20$  regions. In the latter, nearly pure 2p-2h components have been shown to dominate the  $0^+$  ground states [18].

It should be also pointed out that this evolution of the neutron filling and of the particle-hole structure does not mean that the nuclei will become more and more

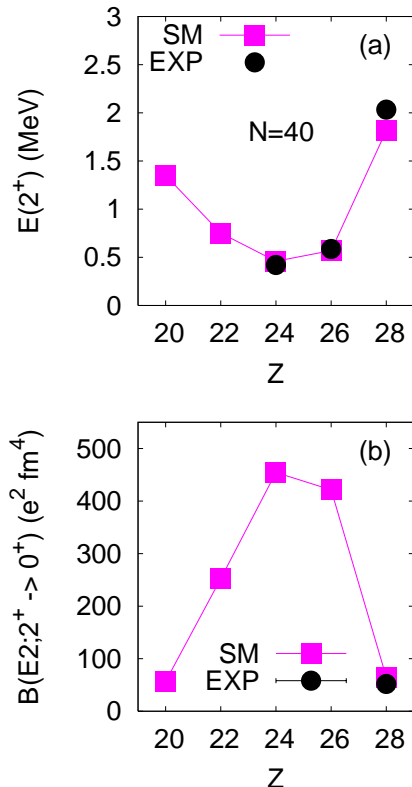


FIG. 2: (Color online) Evolution of the nuclear structure along the  $N = 40$  isotopic chain: (a) theoretical  $2^+$  excitation energies and (b)  $B(E2; 2^+ \rightarrow 0^+)$  values, compared to the available experimental data.

TABLE I: Occupation of the neutron intruder orbitals and percentage of particle-hole excitations across the  $N = 40$  gap in the ground states of the  $N = 40$  isotones. The last column contains the correlation energies evaluated for these states.

Nucleus	$\nu g_{9/2}$	$\nu d_{5/2}$	0p0h	2p2h	4p4h	6p6h	$E_{corr}$
$^{68}\text{Ni}$	0.98	0.10	55.5	35.5	8.5	0.5	-9.03
$^{66}\text{Fe}$	3.17	0.46	1	19	72	8	-23.96
$^{64}\text{Cr}$	3.41	0.76	0	9	73	18	-24.83
$^{62}\text{Ti}$	3.17	1.09	1	14	63	22	-19.62
$^{60}\text{Ca}$	2.55	1.52	1	18	59	22	-12.09

deformed with decreasing  $Z$ ; the ground-state deformation properties result from the total balance between the monopole and the correlation energies (mainly of a proton-neutron character). In Table I, we list also these correlation energies extracted from the multipole Hamiltonian along the  $N = 40$  line. Indeed, the correlation energy, reflecting the deformation, increases from Ni to Cr, where it reaches its maximum, and then diminishes toward Ca. The transition between Ni and Cr is not gradual: The removal of two protons already provokes and abrupt change, from spherical to a strongly deformed prolate shape.

#### IV. THE EVOLUTION OF THE DEFORMATION ALONG THE ISOTOPIC CHAINS

The isotope chains provide a very illustrative picture of the evolution of deformation in this region. In Fig. 3 we show the results obtained for the iron chain. In the panel (a) the excitation energies of the  $2^+$  states are compared to the available experimental data. In panel (b) we show the ratio of the excitation energies  $E(4^+)/E(2^+)$  and  $E(6^+)/E(4^+)$ , which make it possible to recognize whether a nuclear spectrum is close to that of the rigid rotor or not. Let us remind that the perfect rotational limit would require  $E(4^+)/E(2^+)=3.33$  and  $E(6^+)/E(4^+)=2.1$ . Panel (c) depicts the theoretical and experimental  $B(E2)$  transition probabilities along the yrast bands. The measured  $B(E2; 2^+ \rightarrow 0^+)$  values from Ref. [9] are plotted with dots and from Ref. [10] with crosses. Finally, the intrinsic quadrupole moments derived from the calculated spectroscopic ones are shown in part (d). To establish a connection between the laboratory and the intrinsic frames we use the relations:

$$Q_{int} = \frac{(J+1)(2J+3)}{3K^2 - J(J+1)} Q_{spec}(J), \quad K \neq 1, \quad (1)$$

and

$$B(E2, J \rightarrow J-2) = \frac{5}{16} e^2 |\langle JK20 | J-2, K \rangle|^2 Q_{int}^2 \quad (2)$$

for  $K \neq \frac{1}{2}, 1$ .

The same properties are plotted in Fig. 4 for the chromium chain. An excellent agreement with the experiment is found for all excitation energies.

The known  $B(E2)$  transition rates are well reproduced within the error bars as well. Comparing the results for both isotopic chains it can be seen that the onset of deformation occurs at different neutron number. In the chromium chain the intrinsic quadrupole moment stays constant along the yrast the band already at  $N = 38$ . This is one of the fingerprints of a good rotor behavior. The iron isotopes undergo the transition at  $N = 40$ . We have also verified that the intrinsic quadrupole moments obtained from the spectroscopic ones (Eq. (1)) are nearly equal to those obtained from the transition probabilities according to Eq. (2) in  $^{62,64,66}\text{Cr}$  and  $^{66,68}\text{Fe}$ . We obtain a value of  $Q_{int} \sim 150 \text{efm}^2$  in  $^{62,64,66}\text{Cr}$  which corresponds to  $\beta \sim 0.35$ . The deformation of  $^{66,68}\text{Fe}$  is slightly lower, with  $Q_{int} = 145 \text{efm}^2$  ( $\beta \sim 0.3$ ). In the lighter Fe and Cr nuclei, the discrepancies between the calculated quadrupole moments and those obtained in the rotational scheme from the  $B(E2)$ 's are much larger.

Let us further discuss the structure of the calculated states. In Table II we show the occupancies of the neutron intruder orbitals in the ground states of the chromium and iron chains. In the case of the  $0g_{9/2}$  orbit the extra occupancy is reported, i.e. the difference between the value obtained in the configuration mixing

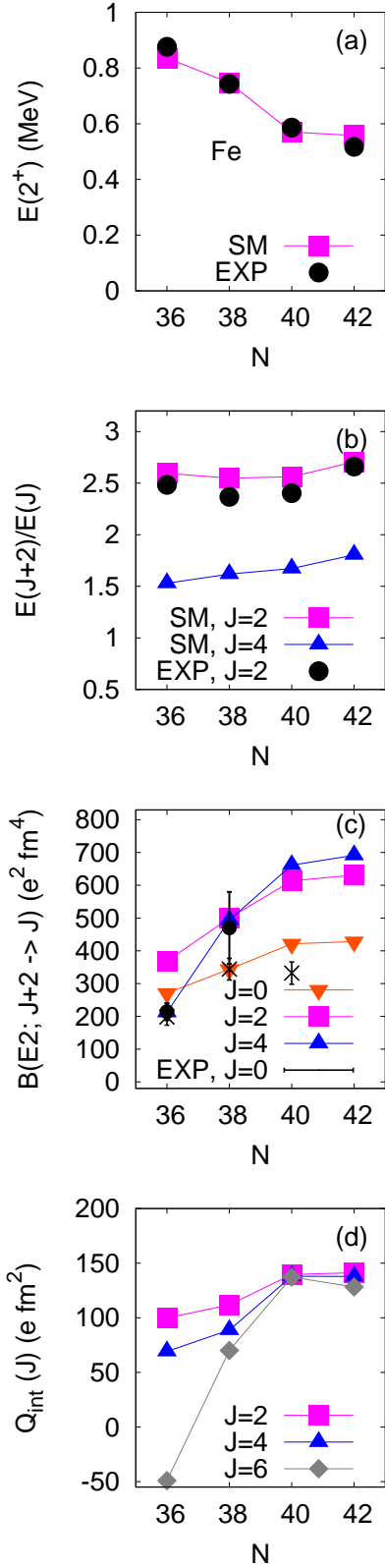


FIG. 3: (Color online) Theoretical results along the iron isotopic chain in comparison with the available experimental data: the excitation energies of the  $2^+$  states are shown in panel (a), in panel (b) we present the ratio of energies of  $E(J+2)/E(J)$ , the  $B(E2)$  transition rates are plotted in panel (c) and the calculated intrinsic quadrupole moments in panel (d). Two experimental sets of the  $B(E2)$  values are shown: from Ref. [9] (black dots) and from Ref. [10] (crosses).

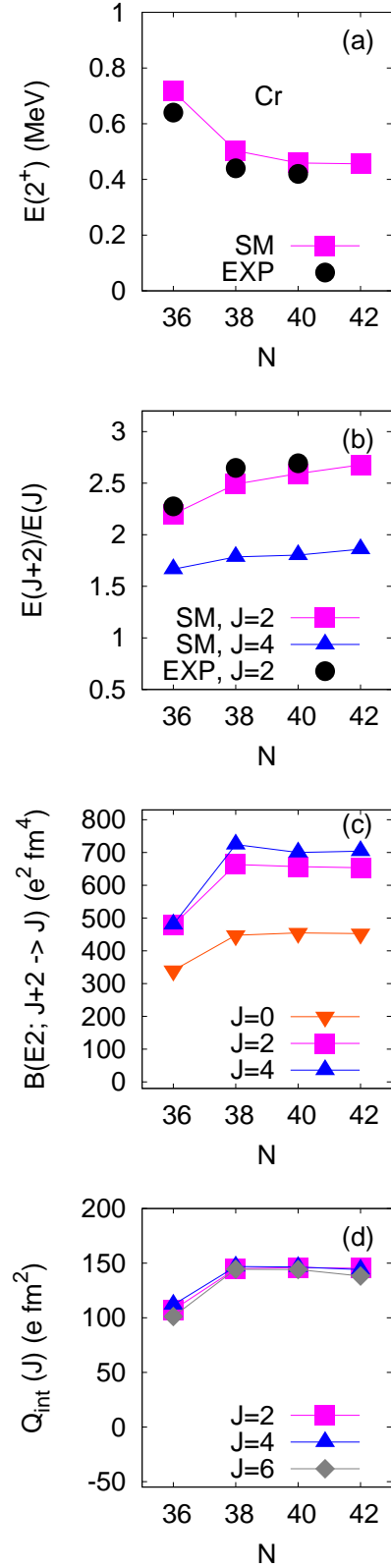


FIG. 4: (Color online) The same as in Fig. 3 but for the chromium isotopes.

TABLE II: Extra occupations of neutron  $0g_{9/2}$  and  $1d_{5/2}$  orbitals in the ground states of the chromium and iron chains.

Nucleus	$N$	$\nu 0g_{9/2}$	$\nu 1d_{5/2}$
$^{62}\text{Fe}$	36	0.95	0.12
$^{64}\text{Fe}$	38	2.0	0.27
$^{66}\text{Fe}$	40	3.22	0.51
$^{68}\text{Fe}$	42	2.30	0.62
$^{60}\text{Cr}$	36	1.55	0.31
$^{62}\text{Cr}$	38	2.77	0.66
$^{64}\text{Cr}$	40	3.41	0.76
$^{66}\text{Cr}$	42	2.28	0.90

calculation and the one that corresponds to the normal filling. The neutron intruder occupations increase with  $N$  in both isotopic chains, however the absolute occupancies are larger in the chromium chain. As mentioned already for the  $N = 40$  nuclei, the strong deformation in the Cr chain is not only due to the increased population of the  $0g_{9/2} - 1d_{5/2}$  doublet, but to the strong proton-neutron correlations which tend to be maximal when four protons are active in the  $pf$  shell as well.

In Fig. 5 we show also the evolution of the collectivity in the nickel chain: in (a) the theoretical energies of the first excited  $2^+$  states are compared with experimental ones, while in (b) we show the calculated transition rates in comparison to the available data. The agreement in the calculated energies is very good for all nickels. Concerning transition rates, the model reproduces well the systematics with the minimum in  $^{68}\text{Ni}$  and the rapid increase of collectivity in  $^{70}\text{Ni}$ . However, the calculated value is closer to the lower tip of the error bar. The transition rate in  $^{64}\text{Ni}$  is underestimated. In this case we know that a better agreement with experiment can be obtained in a full  $pf$  shell calculation as the neutron excitations from  $0f_{7/2}$  orbital are here more important than those through the  $N = 50$  gap and, as expected, the occupation of the  $1d_{5/2}$  orbit remains close to zero in the calculations.

Finally, let us note the recent work on  $^{68}\text{Ni}$  [28], where the excited  $0^+$  states have been investigated and a candidate for a proton 2p-2h intruder has been proposed at an excitation energy of 2.2 MeV. We have calculated the excited  $0^+$  states in our model space and we obtain the first excited  $0_2^+$  state at an energy of 1.2 MeV and the second one  $0_3^+$  at an energy of 2.4 MeV, in good agreement with experiment. The too low excitation energy of the first state can be a result of the delicate mixing between the  $0_1^+$  ground state and the excited  $0_2^+$  state. These two states are characterized by similar proton occupancies with leading 0p-0h (neutron) configuration for the  $0_1^+$  ground state and 2p-2h (neutron) configurations for the  $0_2^+$ . For the  $0_3^+$  state, located at 2.4 MeV, the striking feature is that the dominant proton configuration has exactly two  $0f_{7/2}$  protons less than the ground state, *i.e.* a pure 2p-2h proton configuration.

The total quadrupole sum rules for these states amount

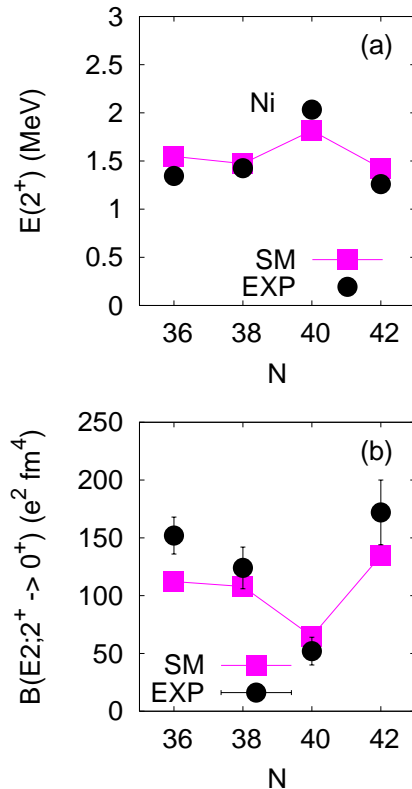


FIG. 5: (Color online) Theoretical versus experimental energies and transition rates of the nickel isotopes in the vicinity of  $N = 40$ .

to 904, 1162 and 2025  $e^2\text{fm}^4$  for the ground state, the  $0_2^+$ , and the  $0_3^+$  states respectively. This shows in particular that the  $0_3^+$  state carries moderate deformation, despite of its proton intruder nature.

## V. CONCLUSIONS

The aim of this work was to study the rapid onset of collectivity below  $^{68}\text{Ni}$ , suggested by the experimental evidence, which is a great challenge for any theoretical model. Here we have presented shell model calculations in a large valence space including the  $pf$  shell for protons and the  $0f_{5/2}$ ,  $1p_{3/2}$ ,  $1p_{1/2}$ ,  $0g_{9/2}$ , and  $1d_{5/2}$  orbitals for neutrons. The effective interaction for this model space has been build up using sets of realistic TBME as a starting point and applying monopole corrections thereafter. The progresses in algorithms and computer power have made it possible to achieve the largest shell model diagonalizations in this region of nuclei up to date.

The present calculations have been performed in Ni, Cr, Fe, Ti and Ca isotopes around  $N = 40$ . We have found a satisfactory agreement between the theoretical results and the available data, for both excitation energies and transition rates. In particular, it has been pos-

sible to describe correctly the rapid onset of collectivity below  $^{68}\text{Ni}$  without any collapse of the spherical gaps.

It has been also shown that the onset of deformation develops at  $N = 40$  in the iron chain and already at  $N = 38$  in chromium isotopes. The maximum deformation is predicted for the chromiums which exhibit features typical of rotational nuclei. The continuous advances in the experimental side, with particular regard to the transition probability measurements, will be a stringent test for these theoretical predictions.

The calculated wave functions of the deformed ground states were shown to contain large amounts of many particle-many hole configurations, with around four neu-

trons occupying intruder orbitals  $0g_{9/2}, 1d_{5/2}$ . We have also related the observed shape change with the underlying evolution of the spherical mean-field, which bears many similarities with the one at the  $N = 20$  *island of inversion*.

**Acknowledgments.** This work is partly supported by a grant of the Spanish Ministry of Science and Innovation MICINN (FPA2009-13377), by the IN2P3(France)-CICYT(Spain) collaboration agreements, by the Spanish Consolider-Ingenio 2010 Program CPAN (CSD2007-00042) and by the Comunidad de Madrid (Spain), project HEPHACOS S2009/ESP-1473.

- 
- [1] D. E. Alburger, C. Chasman, K. W. Jones, J. W. Olness, and R. A. Ristinen, *Phys. Rev.* **136**, B916 (1964).
- [2] C. Thibault, R. Klapisch, C. Rigaud, A. M. Poskanzer, R. Prieels, L. Lessard, and W. Reisdorf, *Phys. Rev. C* **12**, 644 (1975).
- [3] C. Detraz, M. Langevin, D. Guillemaud, M. Epherre, G. Audi, C. Thibault, and F. Touchard, *Nuclear Physics A* **394**, 378 (1983), ISSN 0375-9474.
- [4] E. Caurier, G. Martinez-Pinedo, F. Nowacki, A. Poves, and A. P. Zuker, *Rev. Mod. Phys.* **77**, 427 (2005).
- [5] B. Brown, *Prog. Part. Nucl. Phys.* **47**, 517 (2001).
- [6] T. Otsuka, M. Honma, T. Mizusaki, N. Shimizu, and Y. Utsuno, *Progress in Particle and Nuclear Physics* **47**, 319 (2001), ISSN 0146-6410.
- [7] O. Sorlin et al., *Phys. Rev. Lett.* **88**, 092501 (2002).
- [8] M. Hannawald et al. (ISOLDE), *Phys. Rev. Lett.* **82**, 1391 (1999).
- [9] J. Ljungvall, A. Gorgen, A. Obertelli, W. Korten, E. Clement, G. de France, A. Burger, J.-P. Delaroche, A. Dewald, A. Gadea, et al., *Phys. Rev. C* **81**, 061301 (2010).
- [10] W. Rother et al. (2010), 1006.5297.
- [11] A. Gade et al., *Phys. Rev.* **C81**, 051304 (2010).
- [12] E. Caurier, F. Nowacki, and A. Poves, *Eur. Phys. J.* **A15**, 145 (2002).
- [13] O. Sorlin et al., *Eur. Phys. J.* **A16**, 55 (2003).
- [14] K. Kaneko, Y. Sun, M. Hasegawa, and T. Mizusaki, *Phys. Rev.* **C78**, 064312 (2008), 0812.0205.
- [15] L. Gaudefroy et al., *Phys. Rev.* **C80**, 064313 (2009).
- [16] S. Lunardi et al., *Phys. Rev.* **C76**, 034303 (2007).
- [17] A. P. Zuker, J. Retamosa, A. Poves, and E. Caurier, *Phys. Rev.* **C52**, R1741 (1995).
- [18] Y. Utsuno, T. Otsuka, T. Mizusaki, and M. Honma, *Phys. Rev.* **C60**, 054315 (1999).
- [19] A. Zuker, J. Retamosa, A. Poves, and E. Caurier, *Phys. Rev.* **52**, 9R1741 (1995).
- [20] E. Caurier, private communication.
- [21] M. Hjorth-Jensen, T. Kuo, and E. Osnes, *Phys. Rep.* **261**, 125 (1995).
- [22] F. Nowacki, PhD thesis, IReS Strasbourg (1996).
- [23] S. Kahana, H. C. Lee, and C. K. Scott, *Phys. Rev.* **180**, 956 (1969).
- [24] F. Nowacki and A. Poves, *Phys. Rev. C* **79**, 014310 (2009).
- [25] J. Duflo and A. P. Zuker, *Phys. Rev. C* **59**, R2347 (1999).
- [26] T. Rzaca-Urban, W. Urban, J. L. Durell, A. G. Smith, and I. Ahmad, *Phys. Rev. C* **76**, 027302 (2007).
- [27] E. Caurier and F. Nowacki, *Acta Phys. Pol.* **B30**, 705 (1999).
- [28] D. Pauwels, J. L. Wood, K. Heyde, M. Huyse, R. Julin, and P. Van Duppen, *Phys. Rev. C* **82**, 027304 (2010).